UNIVERSITY OF CALIFORNIA, SAN DIEGO

Using induced pluripotent stem cells and CRISPR/Cas9-mediated targeted mutagenesis to create a model to study Aicardi-Goutières Syndrome

A Thesis submitted in partial satisfaction

of the requirements for the degree Master of Science

in

Biology

by

Leon Lall Tejwani

Committee in Charge:

Alysson R. Muotri, Chair
Yimin Zou, Co-Chair
Jon Christopher Armour

2014

The Thesis of Leon Lall Tejwani is approved, and it is acceptable in quality and form for publication on microfilm and electronically:

_____

_____

Co-Chair

_____

Chair

University of California, San Diego

2014

DEDICATION

I dedicate this thesis to my family for all the support they have provided me during the past twenty-one years of my life. Love you all and hope I am making you proud.

TABLE OF CONTENTS

LIST OF FIGURES

LIST OF TABLES

ACKNOWLEDGEMENTS

I would like to firstly acknowledge Professor Alysson R. Muotri for the opportunity he has given me to be a part of his amazing lab. He and all of the graduate and undergraduate students, post-docs, and lab members have made my experience in the lab better than I could have ever imagined.

Next I would like to thank Yimin Zou and Jon Christopher Armour for not only being on my committee for my thesis, but also their efforts as professors and mentors at UCSD. My experiences in their classes and the knowledge they have imparted upon me have been extremely instrumental in allowing me to find some sort of direction to a future that will truly make me happy.

Last but definitely not least I would like to thank Charles Thomas for pretty much teaching me everything I know about research. Without your effort and support during the past two and half years, I doubt I would be in this position today. Good luck in law school, Charlie.

ABSTRACT OF THE THESIS

Using induced pluripotent stem cells and CRISPR/Cas9-mediated targeted mutagenesis to create a model to study Aicardi-Goutières Syndrome

by

Leon Lall Tejwani

Master of Science in Biology

University of California, San Diego, 2014

Professor Alysson R. Muotri, Chair

Professor Yimin Zou, Co-Chair

Aicardi-Goutières Syndrome is a neurological disease resulting in a variable array of symptoms, of which include microcephaly, calcification of the basal ganglia, leukodystrophy, and other neurological defects, all of which are accompanied by a mild to severe mental handicap seen in patients with the disease. In this disease, there is a

mishandling of nucleic acids due to mutations in one of several nucleases and this mishandling is hypothesized to be involved in an autoimmune response triggered by the anomalous DNA or RNA. In order to better study the effects of these mutations, in particular mutations in three-prime repair exonuclease 1 (TREX1), I have described a method to generate neural progenitor cells, neurons, and astrocytes from induced pluripotent stem cells (iPSCs) and embryonic stem cells (ESCs) to obviate the need to isolate brain tissue from patients or utilize post-mortem brain tissue. By reprogramming AGS1 patient fibroblasts with a V201D mutation into iPSCs and by generating H9 embryonic stem cell wild-type/mutant TREX1 isogenic pairs, along with being able to successful differentiate these pluripotent stem cells into cells of the neural lineage, I have begun to establish an *in vitro* platform that allows for direct observation of the effects of TREX1 mutations on the development and function of various cell types that make up the brain.

Introduction

Aicardi-Goutières Syndrome

Aicardi-Goutières Syndrome (AGS) is a rare, early onset neurodevelopmental disorder with around 200 reported cases around the world.[4] Approximately ninety percent of patients with AGS are seen to have a mutation in a gene coding for one of the following six nucleases-- three-prime repair exonuclease 1 (TREX1; AGS1), the three subunits of ribonuclease H2 (RNASEH2A, RNASE2HB, or RNASE2HC; AGS4, AGS2, and AGS3, respectively), SAM domain and HD domain-containing protein 1 (SAMHD1; AGS5), or adenosine deaminase acting on RNA (ADAR1; AGS6). AGS is typically inherited in an autosomal recessive manner, however the disease has also been seen to arise from *de novo* autosomal dominant mutations in TREX1 or ADAR1, although this situation is unusual.[2]

Given the genetic heterogeneity of AGS the severity of phenotype, types of symptoms, and onset of disease can also appear heterogeneous as well. Generally, clinical diagnosis involves the following symptoms: severe intellectual and physical handicap, calcification of the basal ganglia, particularly of the putamen, globus pallidus, and also thalamus and parts of the white matter (visualized through CT imaging), frontotemporal leukodystrophy, cerebral atrophy, elevated levels of interferon-alpha (IFN-α) in the CSF and serum, progressive microcephaly, and chronic CSF lymphocytosis.[2] In addition to these neurological defects, a common extra-neurological disease marker that is present in 43% of patients is chilblain lesions.[12] While most of these symptoms are involved in diagnosing patients with AGS, some of the listed symptoms may be variable in degree, or even absent, in some AGS patients. Clinically,

there are two main presentations of AGS: neonatal onset with neurological illnesses manifesting themself at birth or after a few days of being born, and a later onset form in which symptoms present after a few months of life.[4] Early-onset AGS is typically associated with mutations in TREX1 and is not only characterized by the neurological defects mentioned previously, but also additional extra-neurological features which include hepatosplenomegaly, elevated transaminases, and thrombocytopenia.[12] The later onset form of AGS typically arises due to mutations in RNASEH2B, and this form is associated with lower mortality and decreased severity of symptoms (compared to earlier onset forms), with patients having relatively preserved intellectual function.[12]

Three-prime repair exonuclease 1 (TREX1) and AGS1

Three-prime repair exonuclease 1 (TREX1), or DNase III, is a single exon gene located at the 3p21.31 locus that encodes a 314-amino acid protein ubiquitously expressed in mammalian cells. As a part of the DnaQ family of 3'→5' exonucleases, a group of structurally conserved proteins spanning from Archaea and bacteria to humans, TREX1 contains three conserved exonuclease motifs that are hallmark to proteins of this family, Exo I, Exo II, and Exo III, which collectively make up the catalytic site.[11,13] TREX1 also contains a highly hydrophobic carboxyl terminus that forms a double-helix that is crucial to the intracellular localization function. However, this domain plays no role in the enzymatic function of TREX1. Additionally, the proline-rich sequence (PPII) is important in the protein-protein interactions of TREX1, in particular, with the SET complex, a protein complex associated with the endoplasmic reticulum to which TREX1 colocalizes to from its perinuclear location and functions in major cell processes such as apoptosis, nucleosome assembly, and histone binding.[7]

As the major 3'→5' exonuclease in mammalian cells, TREX1 is thought to regularly function in the removal of anomalous DNA from the cell with a high specificity for single-stranded DNA (ssDNA) due to its structural properties.[8] Different mutations in TREX1 often result in autoimmune conditions such as Aicardi-Goutières Syndrome, systemic lupus erythamatosus, cerebral leukodystrophy, and retinal vasculopathy. Due to the loss of the normal ability to attenuate immune response caused by persistent ssDNA and double-stranded DNA (dsDNA), cells undergo an autoimmune attack which involves an increase in levels of type I interferons, as seen in most patients.[8] Of the seventeen identified mutations in TREX1 that are implicated as the cause of early neonatal onset AGS (AGS1, OMIM 225750), eleven of the mutations result in null alleles in which the protein is truncated and enzymatic function is devoid, while the remaining mutations result in proteins with diminished enzymatic activity.[12] This decreased enzymatic activity of TREX1 in disease conditions is thought to yield excess ssDNA in the CSF and serum, a phenotype that is characteristic of AGS1 patients.

Reprogramming dermal fibroblasts into induced pluripotent stem cells

For a long time, it had been thought that cells develop unidirectionally—from the pluripotent stem cells that make up the embryo into the differentiated somatic cells that make up the developed tissues found in an adult. Recently however, the concept of reversing this supposedly unidirectional differentiation has been accomplished with the discovery by Shinya Yamanaka of the ability to reprogram differentiated cells into induced pluripotent stem cells. By ectopically expressing specific transcription factors, which include Oct4, Sox2, Klf4, cMyc, now referred to as the "Yamanaka factors", cells can be restored to a pluripotent state, in which they are capable of self-renewal and

differentiation to tissues of the three germ layers, behaving similarly to embryonic stem cells.[9] This ability to "reprogram" differentiated human somatic cells into pluripotent, embryonic stem cell-like cells has emerged as a tool with tremendous utility, especially in the fields of neuroscience and neurology. Due to the limited access to brain tissue from patients with neurological disorders (other than post-mortem brain tissue), this method of producing induced pluripotent stem cells (iPS cells) has revolutionized the ability to study the molecular and cellular pathology seen in the brains of patients with mutation-driven conditions.

Although there are multiple methods that have been developed to achieve this goal of reprogramming differentiated cells into stem cells, the use of nonintegrating, autonomous episomal plasmids to deliver the Yamanaka factors discussed above has proven quite successful in achieving the goal, as it overcomes any limitations emerging from the use of viral vectors for reprogramming, such as integration of the transgene into the host genome.[14] It has been shown that oriP/EBNA1 (Epstein-Barr nuclear antigen-1)-based episomal vectors can be transfected into mammalian cells without the need for viral packaging, resulting in stable extrachromosomal plasmids that require a cis-acting oriP element and a trans-acting EBNA1 gene to replicate.[16] With drug selection, clones with stable episomes can be isolated and upon reprogramming, drug selection can be removed and the episome is gradually lost from the reprogrammed cell due to the progressive loss of the plasmid through generations as the cells proliferate. Upon removal of the episome, the plasmid and the transgene are absent in the successfully reprogrammed cell.[16]

CRISPR technology to create isogenic H9 ESC lines

While there have been multiple artificial nuclease systems used for genome editing such as zinc-finger nucleases (ZFNs) and transcription activator-like effector nucleases (TALENs), a novel technique in gene editing has emerged in the past two years, known as clustered regularly interspaced short palindromic repeats (CRISPR) technology. This technology utilizes components of an acquired immune function of bacteria and archaea against viruses and phages, which consists of CRISPR RNA (crRNA)-based DNA recognition and nonspecific CRISPR-associated (Cas) nucleases to induce DNA cleavage, thereby eradicating invading foreign DNA.[17] In response to invading phage and virus DNA, bacteria and archaea have the ability to degrade the invading DNA and integrate into the CRISPR locus as spacer between the repetitive sequences, and it is later transcribed to produced pre-crRNA. This pre-crRNA is processed by the Cas proteins into small fragments (crRNA) that guide the subsequent cleavage of exogenous DNA and RNA.[10] The CRISPR/Cas system can be classified as type I, II, or II, depending on the structures and sequences of the Cas protein of interest.

The type II CRISPR/Cas system has been particularly useful in genome editing, since its function is simple and only requires a single Cas protein (Cas9). In endogenous CRISPR/Cas9-mediated genome editing specifically, crRNA joins with transactivating crRNA (tracrRNA), forming a tracrRNA:crRNA complex that is able to direct the Cas9 nuclease to the site of interest. For proper cleavage at the target site, a short, three nucleotide protospacer adjacent motif (PAM) and crRNA matching the DNA sequence are required. Upon binding of the Cas9 nuclease to the target site, a double stranded break is induced and the innate cellular DNA repair process is initiated. Error-prone non-homologous end joining or error-free homology domain repair can occur, the former

inducing mutagenesis by random insertions or deletions at the target site desired for perturbing normal gene expression.[6]

Although mammalian cells do not have the innate ability to undergo CRISPR/Cas9-mediated DNA breakdown, researchers have developed technology that allows for a similar process to occur to target particular sites in the human genome. By developing guide RNAs (gRNAs) containing all necessary tracrRNA and crRNA elements to recognize a particular 20-24 nucleotide sequence, along with 2-4 nucleotide PAM sequences near the target site, CRISPR/Cas9 with gRNAs can induce double-stranded breaks at unique regions of the genome.[17] The application of this artificial CRISPR/Cas9 nuclease to human embryonic stem cells to manipulate specific genes by random insertions or deletions has proven successful in creating isogenic pairs of wild-type/mutant cell lines to directly study the result of a mutation in a single gene.

Results

Successful reprogramming of AGS1 patient fibroblasts into induced pluripotent stem cells

After having the Stem Cell Core at Sanford Burnham Medical Research Institute reprogram the AGS1 patient fibroblasts with a V201D mutation **(Fig. 1A),** three clones were successfully selected and expanded for use throughout the course of this project. These clones were assigned the names of A1C1, A1C2, for A1C3 (for AGS1 and clone number). In order to assess the pluripotency of these supposedly reprogrammed cells, several different methods were employed to fully explore different characteristics of truly pluripotent stem cells. Immunocytochemistry was performed to qualify expression of pluripotent markers at the protein level. **(Fig. 1B)** Each of the four clones expressed the two tested markers, Nanog and Lin28. Next, expression of several pluripotent markers was measured at the mRNA level by quantitative real-time polymerase chain reaction (qPCR). TaqMan probes against six pluripotent markers (cMyc, Klf4, Lin28, Nanog, Oct4, Sox2), as well as two endogenous controls (B2M, HPRT1) were used for the analysis. As demonstrated by the quantification cycle (C_q) and standard error of the mean (SEM) values graphed in **Fig.1C**, qPCR showed an overall increase in pluripotent markers Lin28, Nanog, and Sox2 in the induced pluripotent stem cells when compared to fibroblasts. Markers c-Myc, Oct4, and Klf4 showed no apparent trend when comparing the ESCs with the fibroblasts. As a final assessment of pluripotency, the ability for one of the selected iPSC clones to differentiate into cells of each of the three germ layers was examined by immunostaining of teratomas formed in mice. As seen in **Fig. 1D**, iPSCs from A1C1 successfully differentiated into endoderm (left), mesoderm (middle),

ectoderm (right). Finally, the karyotypes of A1C1, A1C2, and A1C3 were examined and shown to have no major abnormalities post-reprogramming **(Fig. 1E).**

Generating isogenic pairs of wild-type and mutant TREX1 pluripotent stem cells from H9 embryonic stem cells and characterization of their pluripotency

H9 embryonic stem cells were transfected with plasmids to co-deliver Cas9 nuclease and either one of two guide RNAs (gRNAs), here labeled gRNA5 and gRNA6, to induce random insertions and deletions at two particular sites in the ESC TREX1 gene depending on which gRNA was used. Transfected cells were plated as single cells and the colonies that formed from each cell were selected and grown individually in separate plates. After proliferating, genomic DNA from each clone was isolated and the CRISPR locus was amplified by polymerase chain reaction (PCR). The PCR product was run on an agarose gel and images of the products were examined to preliminarily detect possible insertions and deletions (image not shown). Next, sequencing of the amplified TREX1 product from each clones was performed. Finally, TOPO cloning and additional sequencing were performed to ensure homozygous mutagenesis for several clones. The gel results, and sequencing results are summarized in **Table 1** (gRNA5) and **Table 2** (gRNA6). Clones 517 and 521 for gRNA5 and Clones 604 and 612 for gRNA6 were selected for further expansion.

Pairs of isogenic WT/MT pairs were selected base on homozygosity, quality of sequencing data, and ability to grow as pluripotent stem cells. Sequencing data of H9 untransfected cell genomic DNA compared to the WT/MT pairs for the two CRISPR gRNAs **(Fig. 2A, 2B)** confirm a successful frameshift mutation in each of the two sites. In **Fig. 2A**, sequencing data shows insertion of a G nucleotide resulted in a frameshift

mutation, converting V63 into glycine and resulting in a premature stop codon at amino acid positions 100 and 101. In **Fig. 2B**, insertion of an A nucleotide resulted in a frameshift mutation, converting I84 into aspartate and resulting in a premature stop codon at amino acid positions 100 and 101.

Colonies from each of the isogenic pairs, as well as untransfected H9 ESCs were expanded for use for the duration of this project. Similarly to the iPSCs used in this project, characterization of pluripotency was performed using immunocytochemistry and qPCR. All ESCs (H9 untransfected and two pairs of WT/MT TREX1 ESCs) expressed Nanog and Lin28 at the protein level **(Fig 2C)**. Assessment at the mRNA level by qPCR showed an overall increase in pluripotent markers Lin28, Nanog, Oct4, and Sox2 in the transfected and untransfected embryonic stem cells when compared to fibroblasts. Markers c-Myc and Klf4 showed no apparent trend when comparing the ESCs with the fibroblasts. **(Fig. 2D).** Karyotyping was performed on the lines and a normal karyotype was seen for each line (**Fig. 2E**).

Differentiation of AGS patient iPSCs and H9 isogenic embryonic stem cells into cells of the neural lineage

The pluripotent cells discussed above (iPSC clones from AGS1 patient and H9, isogenic embryonic stem cells) were used for differentiation into neural progenitor cells and selected NPCs were differentiated further into neurons and astrocytes. The protocol for differentiation is displayed in **Fig. 3A**. Pluripotent stem cells colonies were overgrown for two days in mTeSR then differentiation began by changing the media to DMEM/F12 with glutamine, penicillin streptomycin (pen-strep), HEPES, and N2 neuroplex with dorsomorphin and small molecule SB431542 for two days. Colonies were

lifted into suspension and placed on a rotary shaker for embryoid body (EB) formation for one week. EBs were plated on matrigel and cultured the media was changed to DMEM/F12 with glutamine, pen-strep, HEPES, N2 neuroplex, GEM21, and bFGF. Neuroectodermal rosettes were formed and mechanically picked and passed to poly-ornithine/Laminin plates after one week. A secondary picking for neuroectodermal rosettes was performed after four days. Prior to plating, these rosettes were dissociated to allow separation of single neural progenitor cells (NPCs) that made up the rosettes. NPCs were expanded and FGF treatment was lifted in order to begin neuronal differentiation. Differentiation of NPCs into neurons lasted for thirty days in N2/Gem21 media. The mixed culture of neurons was purified by FACS for $CD44^{-}/CD184^{-}/CD24^{+}$ and these cells were plated in poly-ornithine/Laminin coated 96-well plates for use in the subsequent experiments. Differentiation into astrocytes was as follows: NPCs grown to confluency, lifted into suspension in NGF at shaken at 90rpm. Media was changed to NG and ROCK inhibitor on day 3, to NG on day 5, and to AGM on day 8. Neurospheres were remained in suspension in AGM, and plated onto poly-ornithine/Laminin on day 21. AGM was changed every 3 days. Astrocytes were isolated after emerging from beneath the neurospheres.

Fig. 3B shows the immunocytochemistry of neuroectodermal rosettes containing NPCs that arose from the plated EBs. Cells were positive at the protein level for the two NPC markers that were tested—Nestin and Sox2. Additional characterization was performed to test for NPC markers at the mRNA level by qPCR on various lines of NPC lines that were developed. TaqMan probes against two endogenous controls (B2M and HPRT1) and six additional markers (Nestin, Sox1, Sox2, Pax6, Oct4, and Ms1) were

used for qPCR and the C_q results were plotted. Each of the NPC samples (except for WT63-3) had higher expression of NPC markers Musashi1, Nestin, and Pax6 when compared to H9ESC expression. H9 ESCs had significantly higher levels of pluripotent marker POU5F1 (Oct4) expression than each of the NPC samples **(Fig. 3C)**. In **Fig. 3D** immunocytochemistry for differentiated astrocytes was performed to detect expression of GFAP (green), vimentin (red), S100β (magenta) at the protein level. As seen in the images, the number of $GFAP^+$ cells made up a small portion of the total cell population. Morphology and size of astrocytes varied greatly within cultures. **Fig. 3E** shows characterization of purified neurons by immunocytochemistry against neuronal markers Map2 (green) and Syn1 (red). Neurons with mutations in TREX1 were seen to be morphologically different than those expressing wild-type TREX1, as shown by the dapi and Map2 stain.

Analysis of AGS nucleic acid (increased ssDNA) phenotype of various cell types with wild-type or mutant TREX1

Differentiatied neural progenitor cells, and astrocytes were immunostained to detect single stranded DNA (white) and markers for their state (Nestin and GFAP, respectively; green). Ten 100x fluorescence images were captured for each cell line and ssDNA puncta were quantified. Examples of images used for ssDNA quantification for NPCs **(Fig. 4B)** and astrocytes **(Fig. 4C)** are shown. Quantification for levels of ssDNA puncta in NPCs was graphed in **Fig. 4A**. NPC lines expressing mutant TREX1 showed increased levels of ssDNA when compared to their isogenic counterparts expressing wild-type TREX1. NPCs with the V63fs mutation treated with reverse transcriptase inhibitors showed lower levels of ssDNA when compared to the untreated V63fs NPCs.

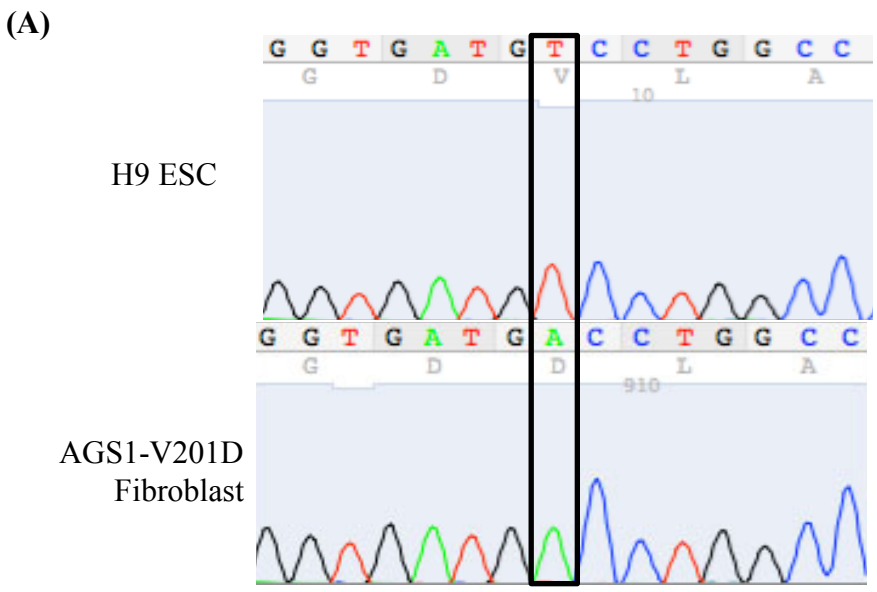

Figure 1. Characterization of pluripotency of induced pluripotent stem cells from reprogrammed AGS patient dermal fibroblasts

(A) DNA sequencing data of the 201 amino acid position of the TREX1gene of H9 embryonic stem cells (top) and AGS1 patient fibroblasts with a thymine→adenine substitution, resulting in a V201D mutation (bottom). The mutation induced conversion of amino acid valine (nonpolar) into aspartate (positively charged).
(B) Immunocytochemistry of four clones (A1C1, A1C2, A1C3) selected from reprogrammed AGS1 patient fibroblasts. Immunostaining for pluripotent markers including Nanog (green) and Lin28 (red), as well as the nuclear dapi stain (blue) was performed.
(C) Real-time quantitative polymerase chain reaction of AGS patient iPSC clones to characterize pluripotency (RT-qPCR). TaqMan probes against pluripotent markers Sox2, POU5F1 (Oct4), Klf4, Nanog, and Lin28 as well as endogenous controls HPRT1 and B2M were used and C_q values for each of the four clones and for AGS1 patient fibroblasts were measured.
(D) H&E teratoma immunohistochemistry to further characterize pluripotency. Mice injected with A1C1 V201D iPSCs formed teratomas containing cells of endoderm (left), mesoderm (middle), ectoderm (right).
(E) Karyotypes of patient-derived iPSC clones A1C1, A1C2, and A1C3.

(B)

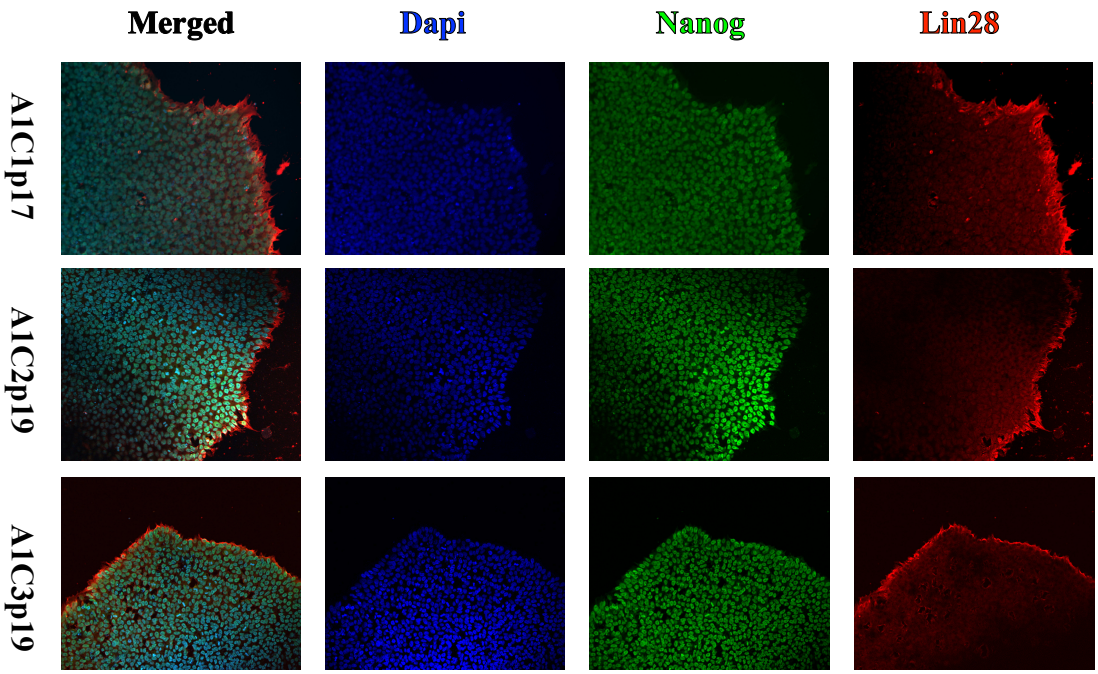

Figure 1. continued

(C)

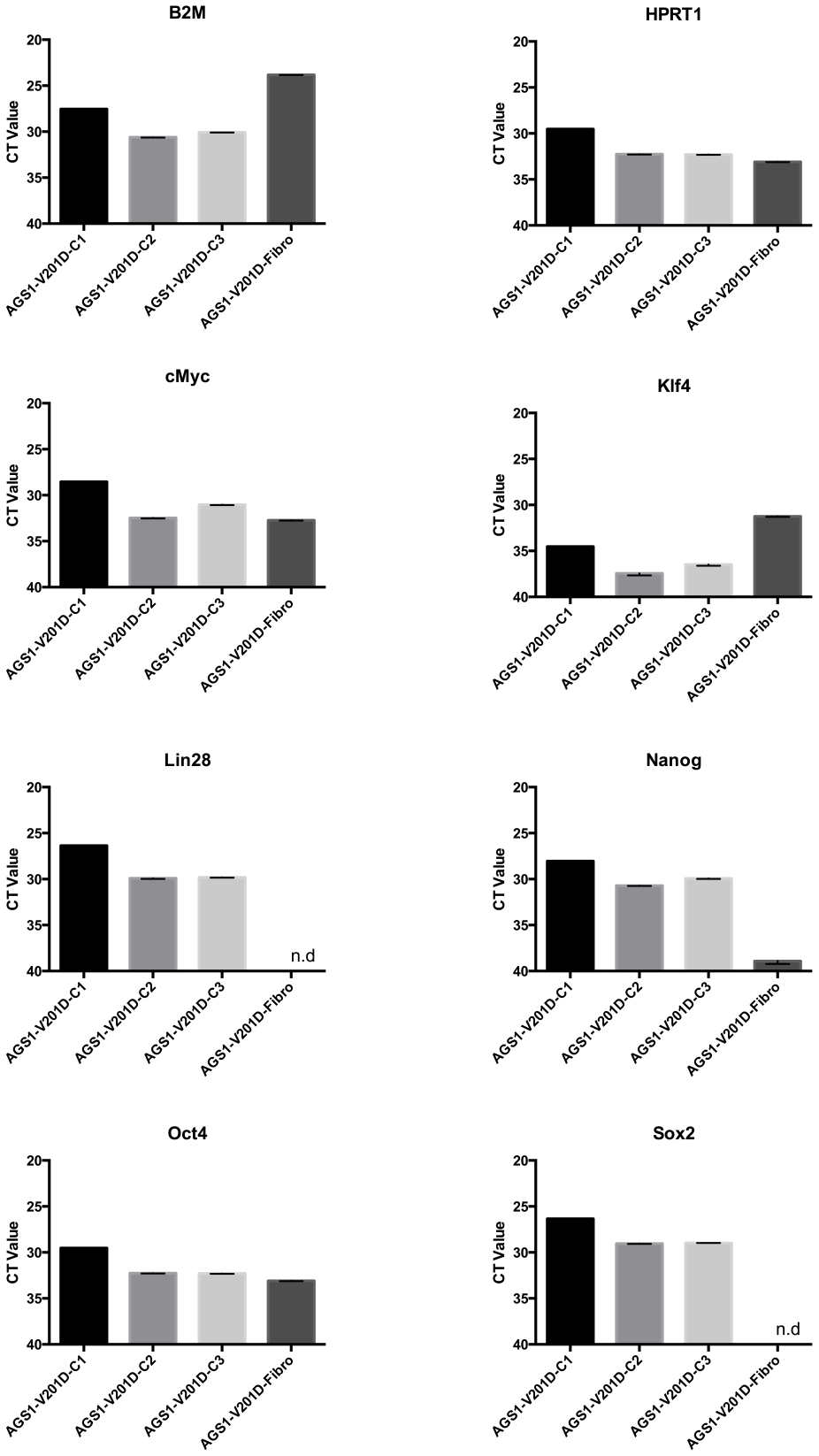

Figure 1. continued

(D)

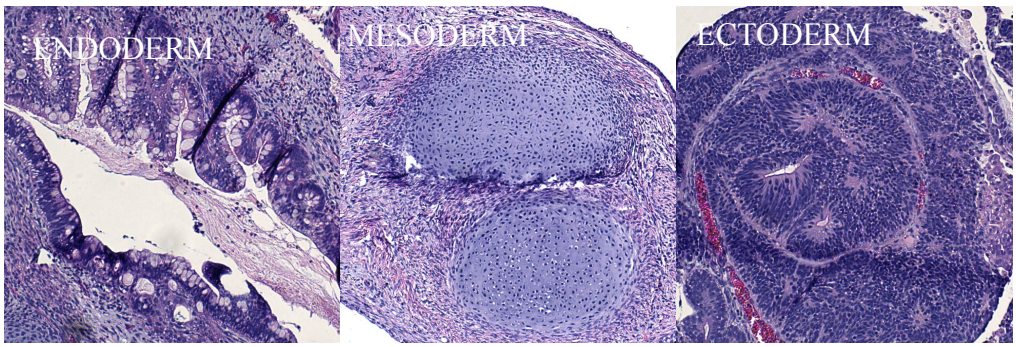

(E)

AGS1-V201D-1

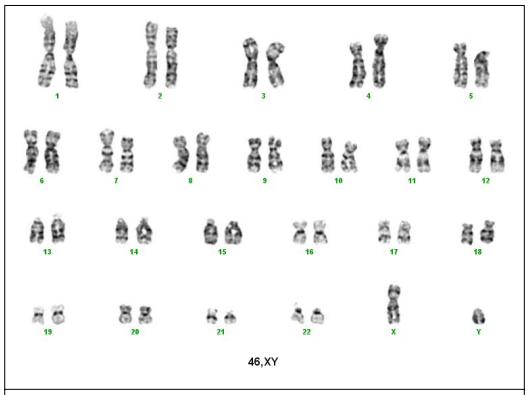

AGS1-V201D-2

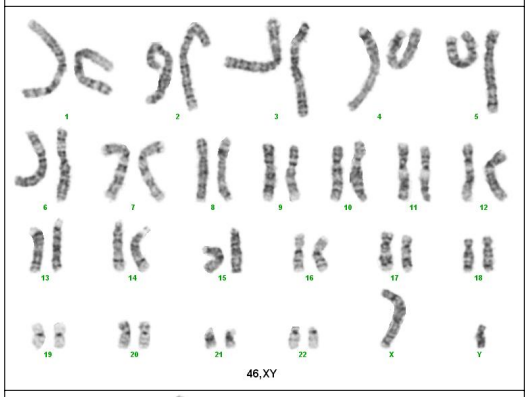

AGS1-V201D-3

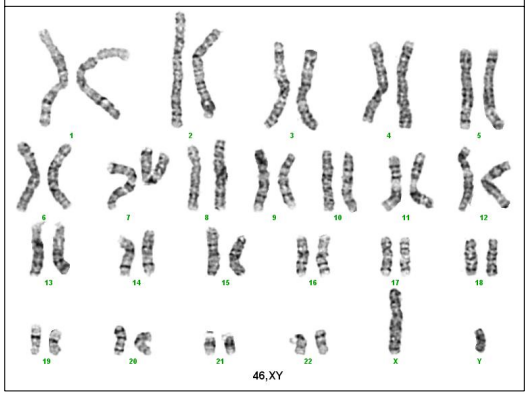

Figure 1. continued

Table 1. Selection of embryonic stem cells from cells transfected with plasmid expressing Cas9/CRISPR gRNA5

Table summarizing results used for selecting isogenic pairs including gel results of amplified TREX1 gene, sequencing results of the gRNA5 locus from this amplified region, and the sequencing results from TOPO cloning. The 517 clone showed a +G insertion in both alleles (+G/+G) and the 521 clone had no mutations detected in either allele (WT/WT). These two clones were selected as isogenic WT/MT counterparts for further expansion and experimentation and the other clones were cryogenically frozen down.

Clone	Gel Result	Seq Result	Topo Clone?	Topo Result
H9		No Mut	Yes	WT/WT
501		No Mut		
502	Ins & Del	13 bp Del		
503		No Mut		
504		Fail		
505		Single Seq		
506		-GT Del		
507		Noisy		
508		-GT Del	Yes	-GT/-GT
509	Ins	Fail		
510	Ins?	Single Seq	Yes	-GT/+G
511	Ins	No Mut		
512		Noisy		
513		+G Ins	Yes	WT/+G
514		Single Seq		
515		Noisy		
516		Noisy	Yes	-TG/+G
517	**Ins?**	**+G**	**Yes**	**+G/+G**
518	Del?	Single Seq		
519		Single Seq		
520	Ins	Noisy		
521		**No Mut**	**Yes**	**WT/WT**
522		+G Ins	Yes	+G/+G
523		Noisy		
524		Fail		
525		Single Seq		
526		Noisy		
527	Ins	Noisy		
528	Del	Single Seq		
529		Fail		
530		Single Seq		
531	Ins	Single Seq		
532	Ins	Fail		
533		-GT Del		
534		+GTG Ins		
535		Single Seq		
536		+GTG Ins		

Table 2: Selection of embryonic stem cells from cells transfected with plasmid expressing Cas9/CRISPR gRNA6

Table summarizing results used for selecting isogenic pairs including gel results of amplified TREX1 gene, sequencing results of the gRNA5 locus from this amplified region, and the sequencing results from TOPO cloning. The 604 clone showed a +A insertion in both alleles (+A/+A) and the 612 clone had no mutations detected in either allele (WT/WT). These two clones were selected as isogenic WT/MT counterparts for further expansion and experimentation and the other clones were cryogenically frozen down.

Clone	Gel Result	Seq Result	Topo Clone?	Topo Result
H9		No Mut	Yes	WT/WT
601	Ins	Noisy	Yes	-GA/+A
602		No Mut		
603		No Mut		
604		**+A Ins**	**Yes**	**+A/+A**
605		No Mut		
606		+A Ins		
607	Del	-10bp Del	Yes	-10bp/-10bp
608				
609		Fail		
610		Single Seq		
611	Del	Single Seq		
612		**No Mut**		
613		No Mut		
614		No Mut		
615		No Mut		
616	Ins	Noisy		
617		Noisy	Yes	-GA/+A
618	Ins	+A Ins		
619	Del	-12Del +3 Ins		
620		Fail		
621	Del	Single Seq		
622		Single Seq		
623		No Mut		
624		Noisy		
625		-15bp Del		
626	Ins	Single Seq		
627		Single Seq		
628		Single Seq		
629		Fail		
630	Ins	-2Del + 22 Ins	Yes	-2Del +100Ins/-2Del +100Ins

(A)

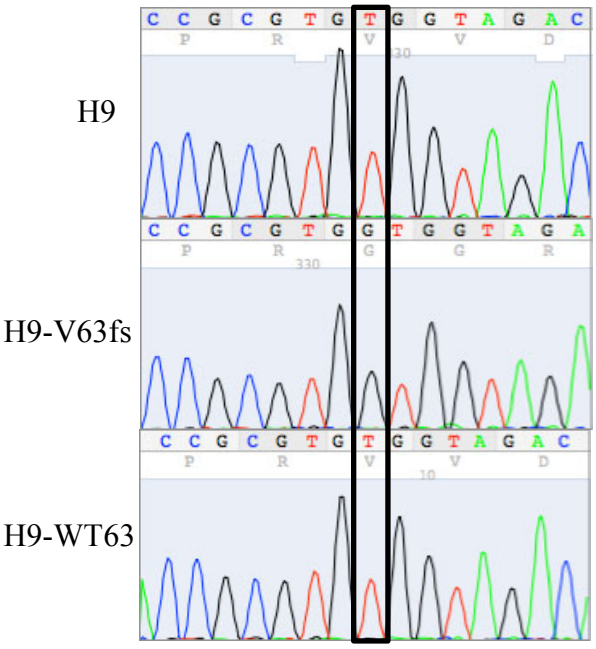

Figure 2. Generation of isogenic pairs of wild-type and mutant TREX1 pluripotent stem cells from H9 embryonic stem cells using CRISPRs

(A) DNA sequencing data of the gRNA5 target site of the TREX1 gene of H9 embryonic stem cells (top), clone 517 with a frameshift mutation at valine amino acid position 63 (V63fs, middle), and clone 521 with no mutations (bottom).

(B) DNA sequencing data of the gRNA6 target site of the TREX1 gene of H9 embryonic stem cells (top), clone 604 with a frameshift mutation at glutamate amino acid position 83 (E83fs, middle), and clone 612 with no mutations (bottom).

(C) Immunocytochemistry of selected CRISPR-induced isogenic pairs of WT/MT TREX1 H9 embryonic stem cells and untransfected H9s to characterize pluripotency. Immunostaining for pluripotent markers including Nanog (green) and Lin28 (red), as well as the nuclear dapi stain (blue) was performed.

(D) Real-time quantitative polymerase chain reaction (RT-qPCR) of embryonic stem cell lines (H9 untransfected, 517, 521, 604,612) clones to characterize pluripotency. TaqMan probes against pluripotent markers Sox2, POU5F1 (Oct4), Klf4, Nanog, and Lin28 as well as endogenous controls HPRT1 and B2M were used and C_q values for each of the lines and for AGS1 patient fibroblasts were measured.

(E) Karyotypes of CRISPRCas9-derived clones H9 untransfected, 517, 521, 604 and 612.

(B)

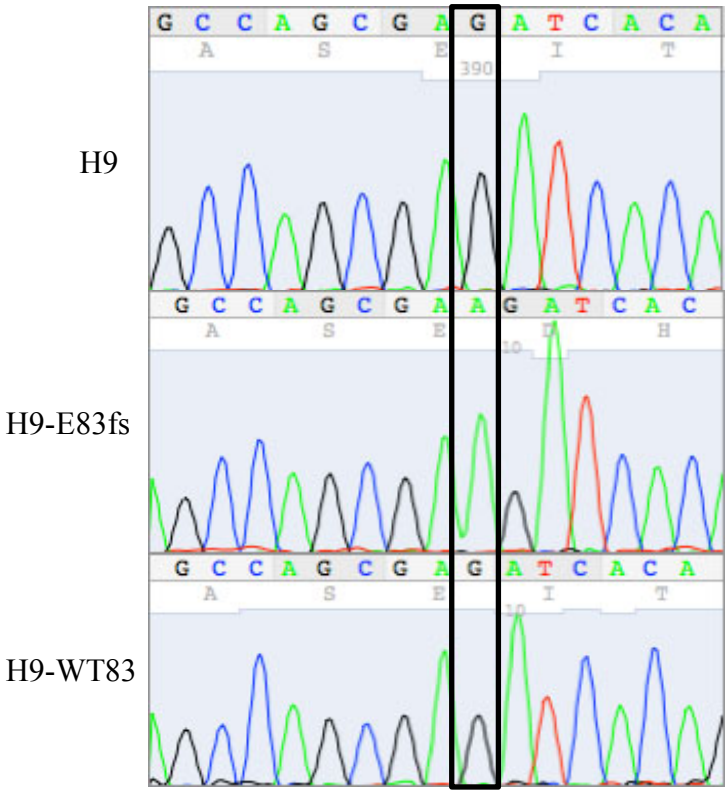

Figure 2. continued

(C)

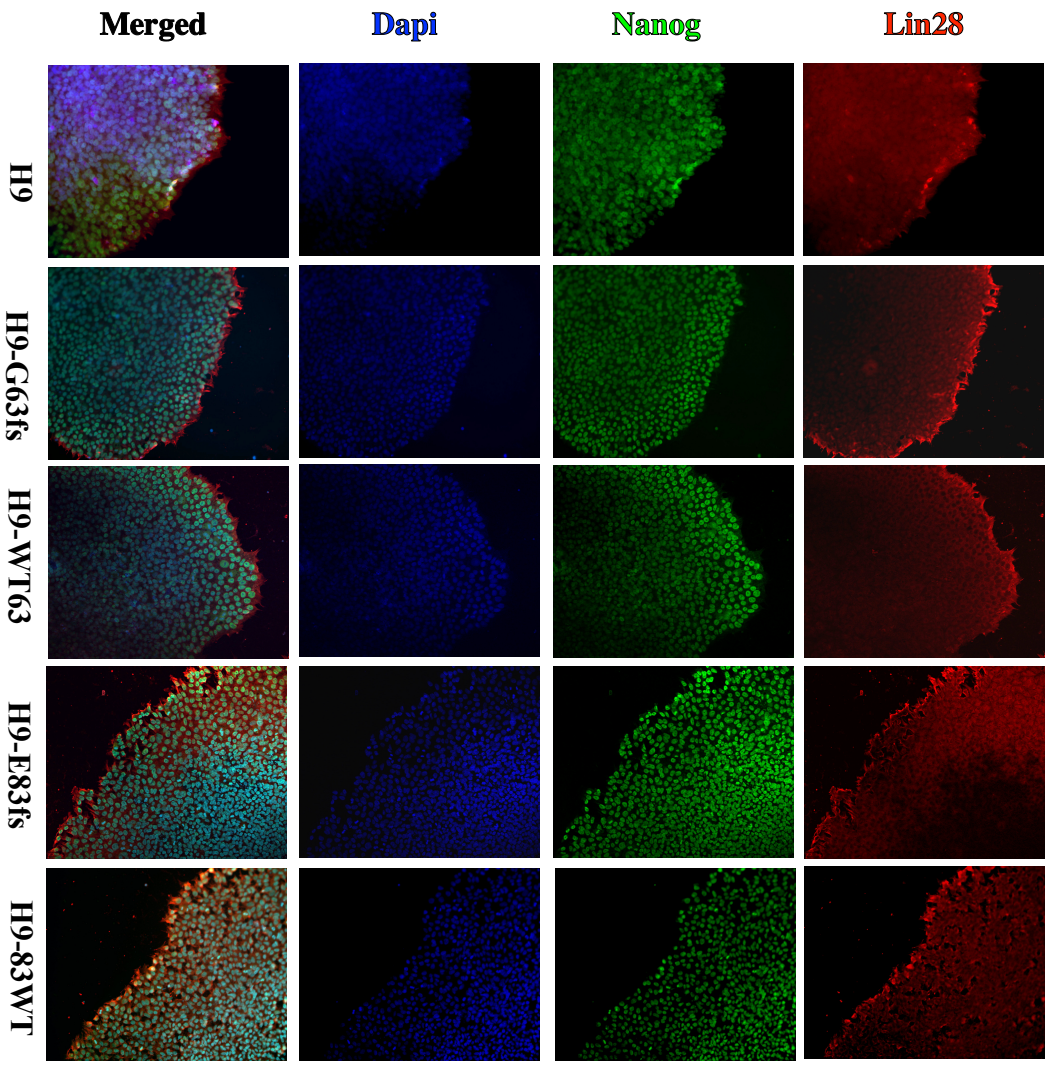

Figure 2. continued

(D)

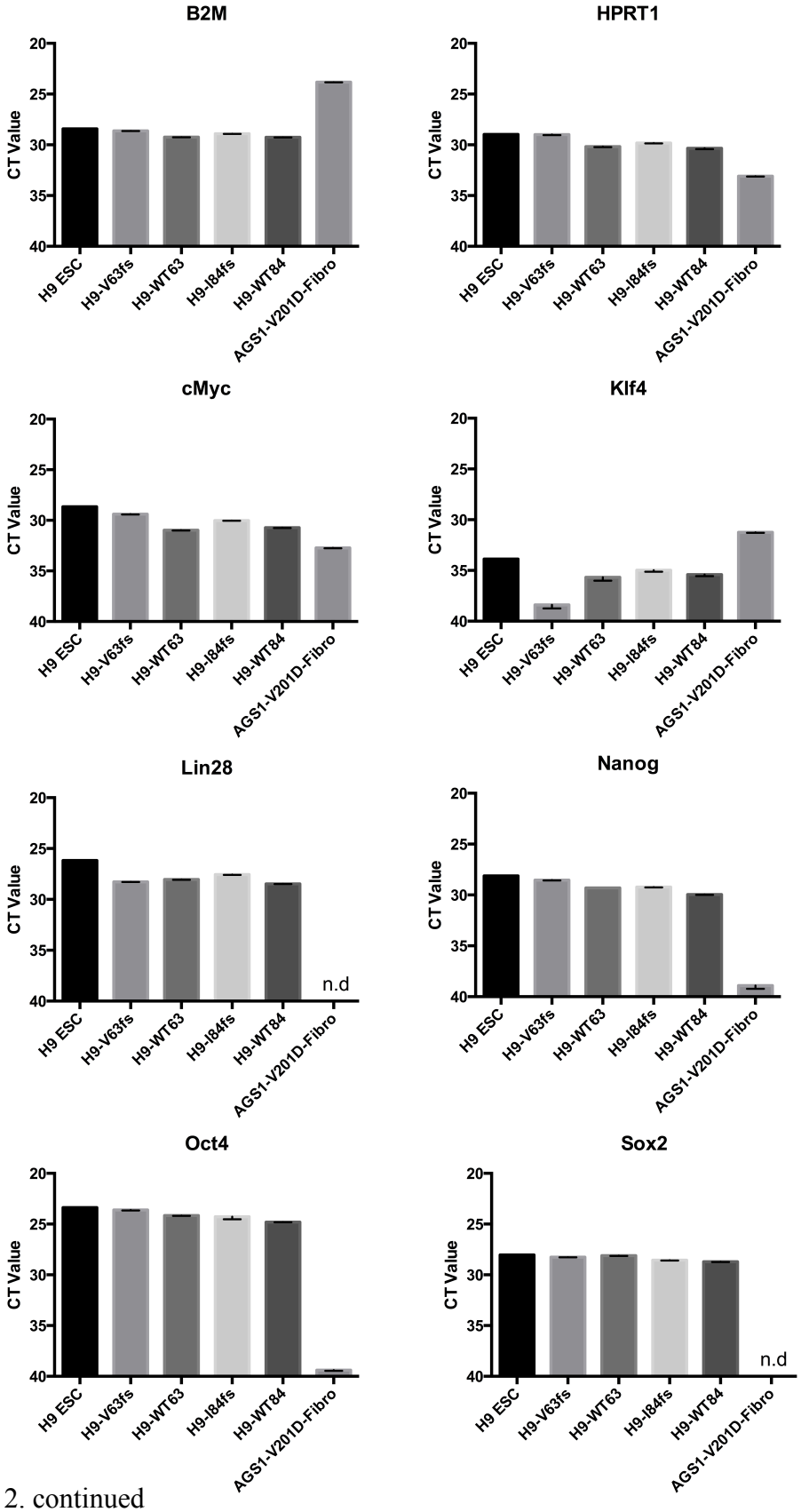

Figure 2. continued

(E)

H9

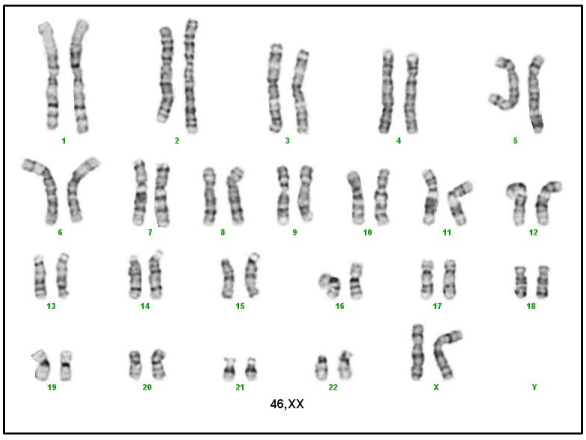

H9-G63fs

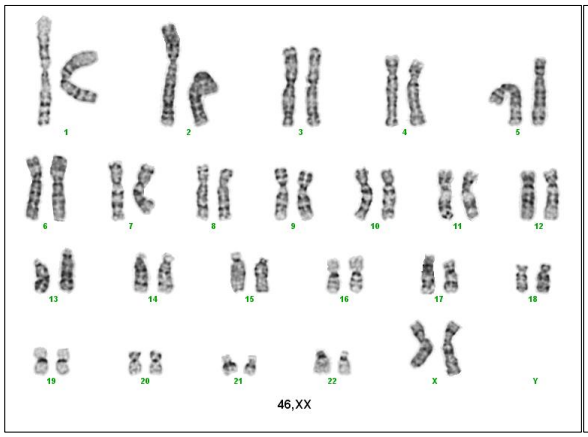

H9-WT63

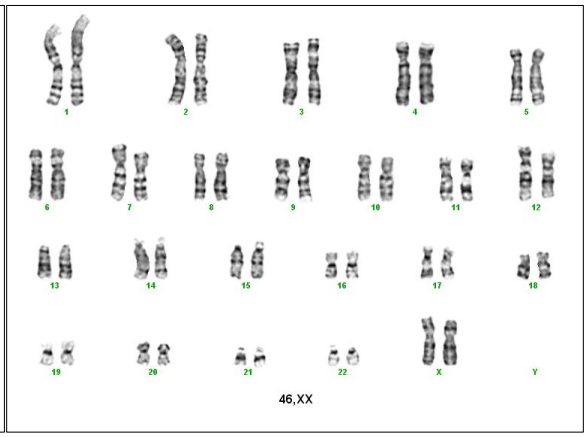

H9-E83fs

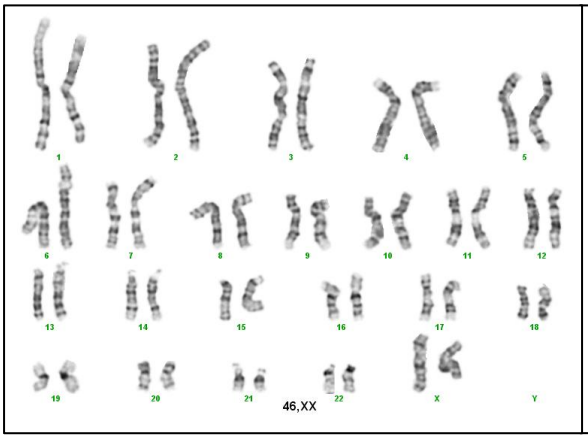

H9-WT83

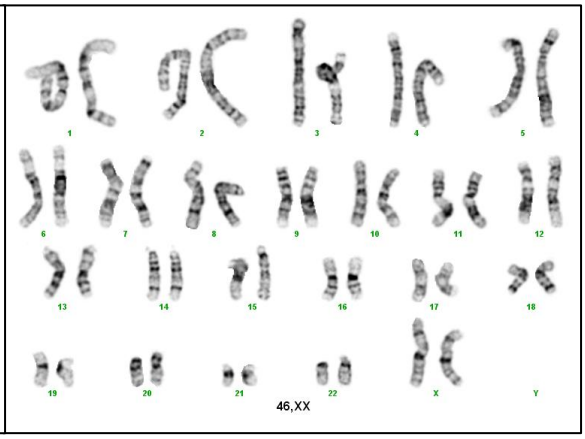

Figure 2. continued

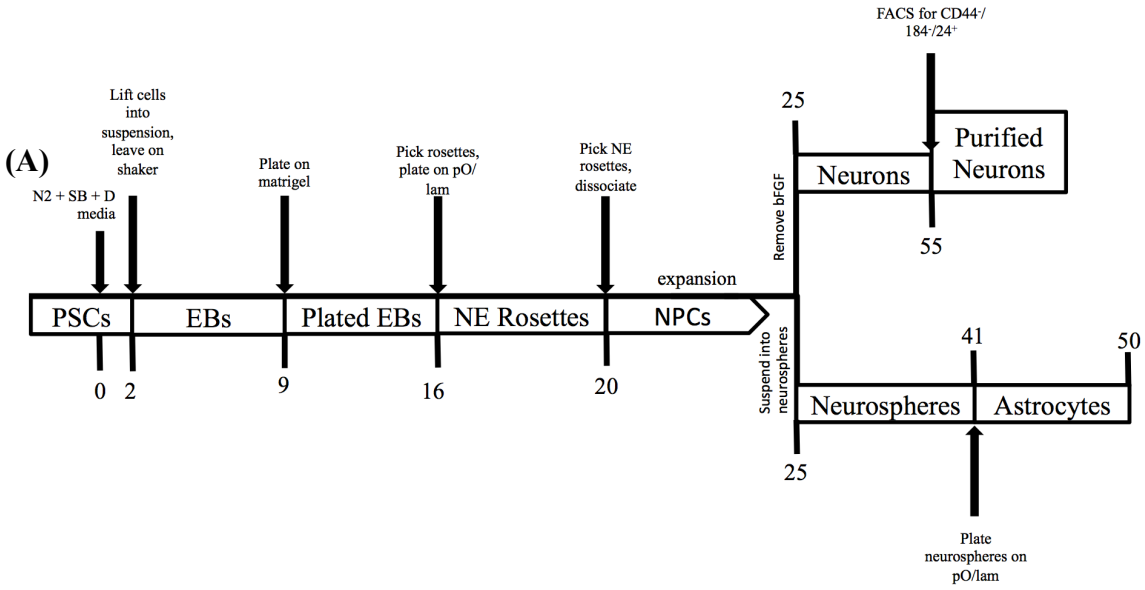

Figure 3. Differentiation of AGS patient iPSCs and H9 isogenic embryonic stem cells into cells of the neural lineage

(A) Schematic for differentiation of pluripotent stem cells (iPSCs and ESCs) into neural progenitor cells, neurons, and astrocytes.

(B) Immunocytochemistry of neuroectodermal rosettes from selected pluripotent stem cells lines to characterize the neural progenitor cell state of the cells making up the rosette. Immunostaining for NPC markers including Nestin (green) and Sox2 (red), as well as the nuclear dapi stain (blue) was performed.

(C) Real-time quantitative polymerase chain reaction of the differentiated neural progenitor cells were performed to characterize the NPC state of the cells. TaqMan probes against NPC markers Sox1, Sox2, Oct4, Ms1, Nestin, and Pax6 as well as endogenous controls HPRT1 and B2M were used and CT values for each of the lines and for AGS1 patient fibroblasts were measured.

(D) Immunocytochemistry of astrocytes differentiated from selected neural progenitor cell lines to characterize the astrocyte state of the cells. Immunostaining for astrocyte markers including GFAP (green), Vimentin(red), and S100β(magenta), as well as the nuclear dapi stain (blue) was performed.

(E) Immunocytochemistry of neurons differentiated from selected neural progenitor cell lines to characterize the neuronal state of the cells. Immunostaining for neuronal markers including Map2 (green) and Syn1(red), as well as the nuclear dapi stain (blue) was performed for H9, H9-WT83, H9-V63fs, and H9-V63fs treated with reverse transcriptase inhibitors (RT_i).

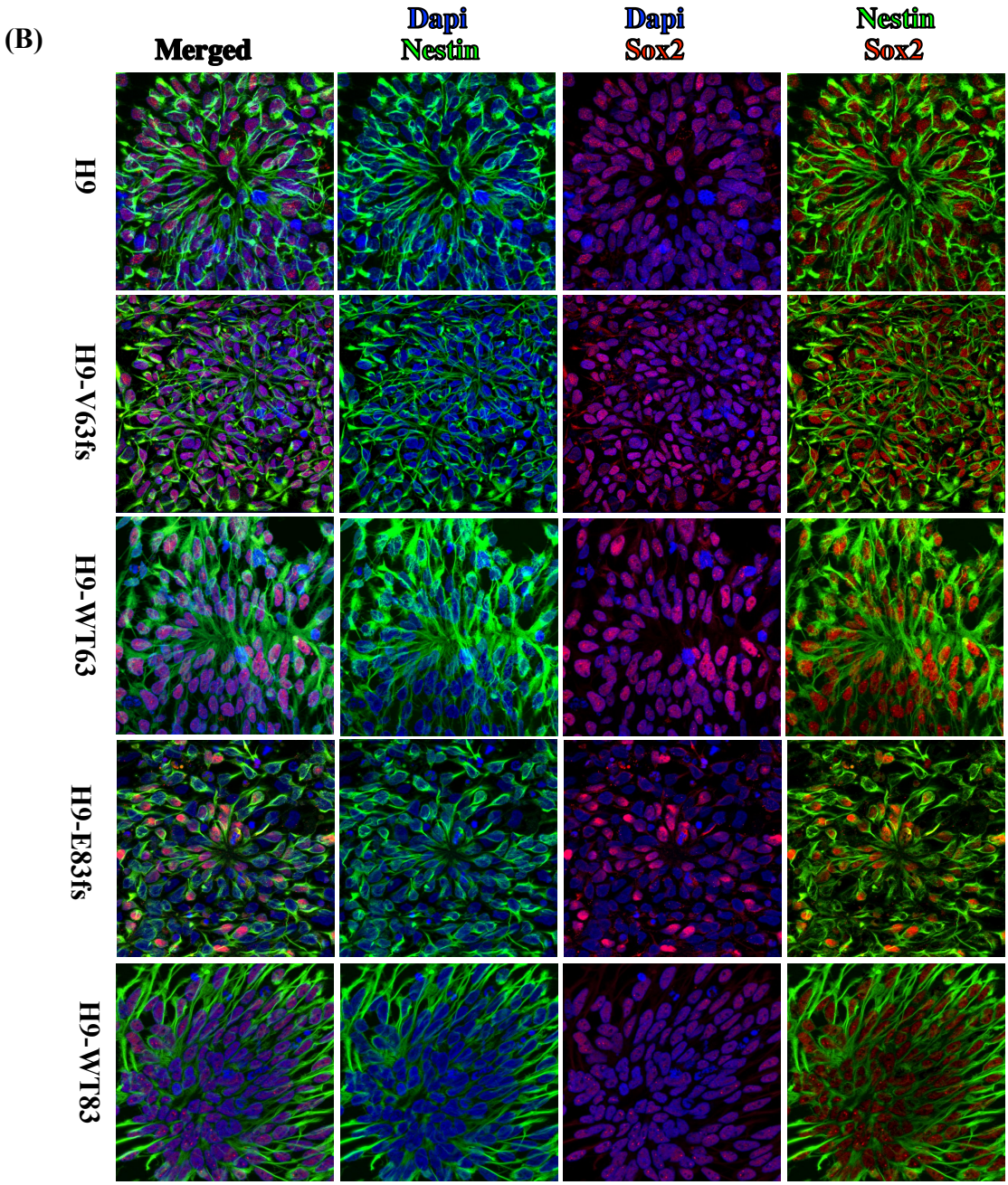

Figure 3. continued

(B continued)

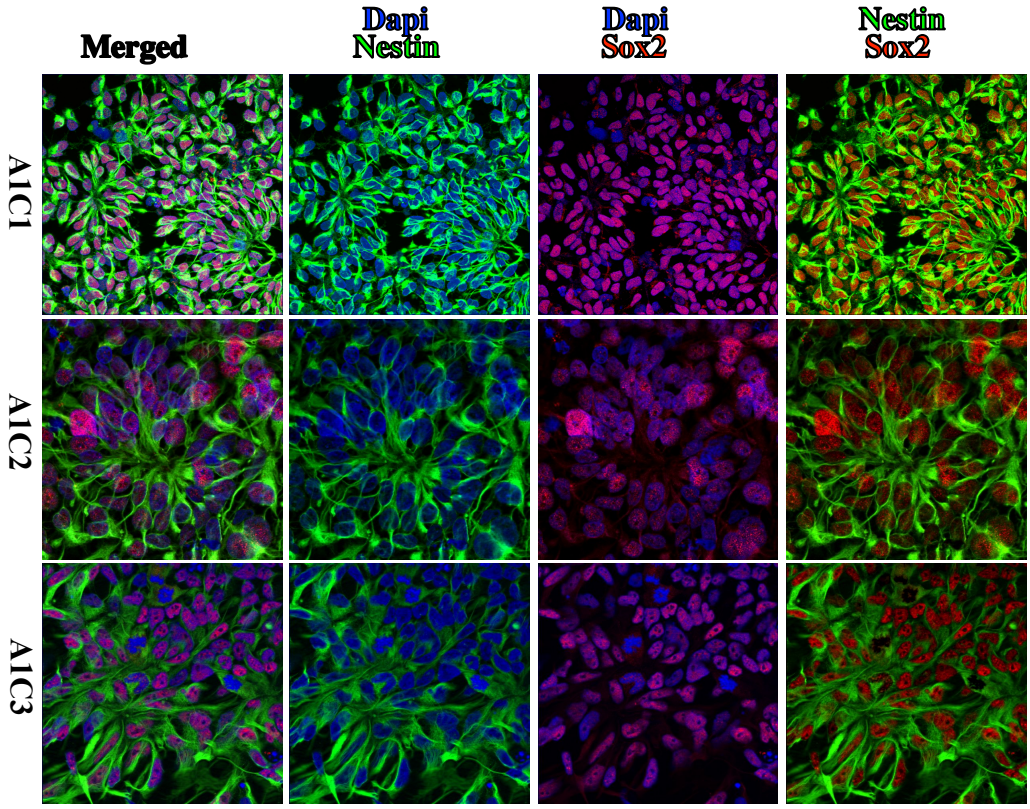

Figure 3. continued

(C)

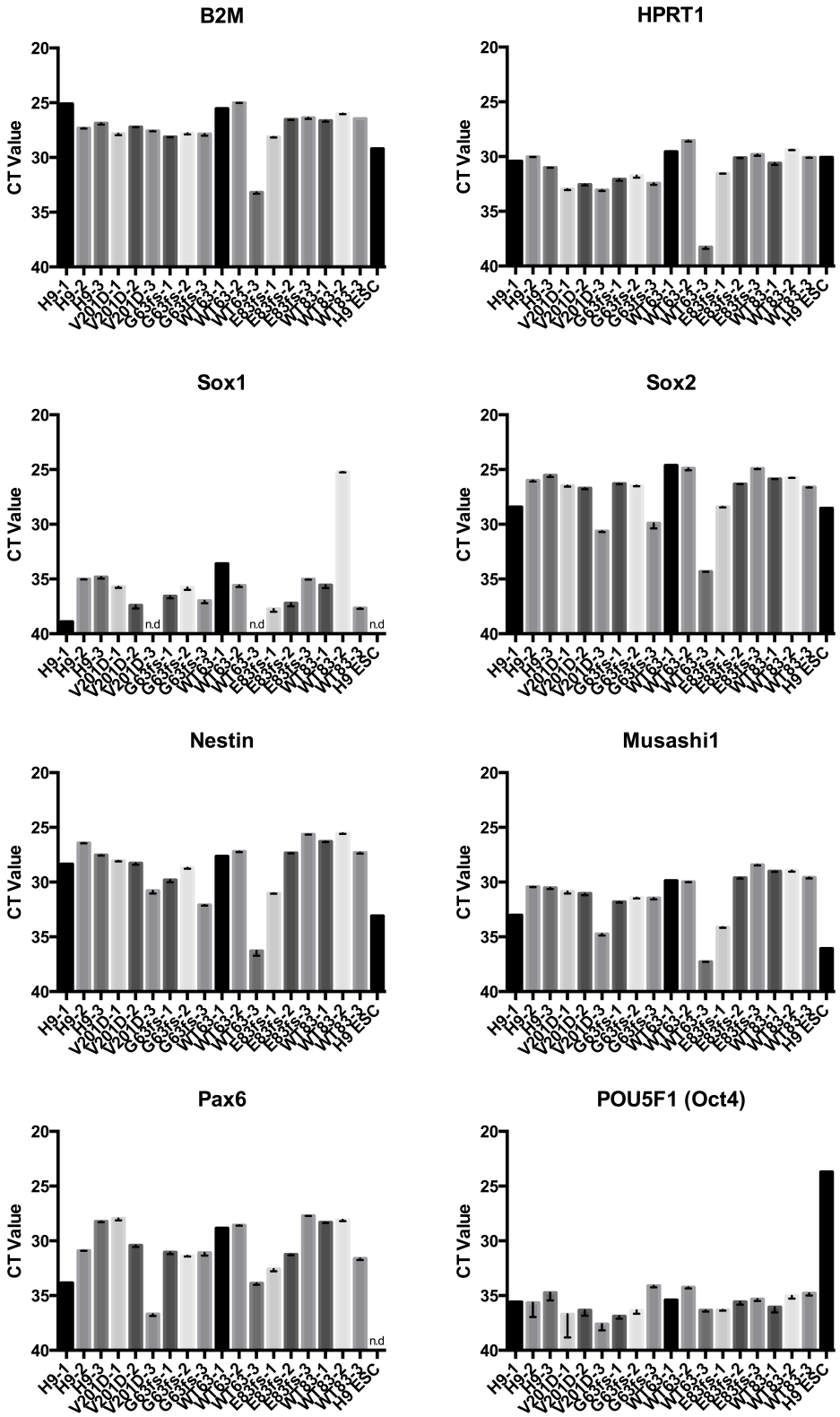

Figure 3. continued

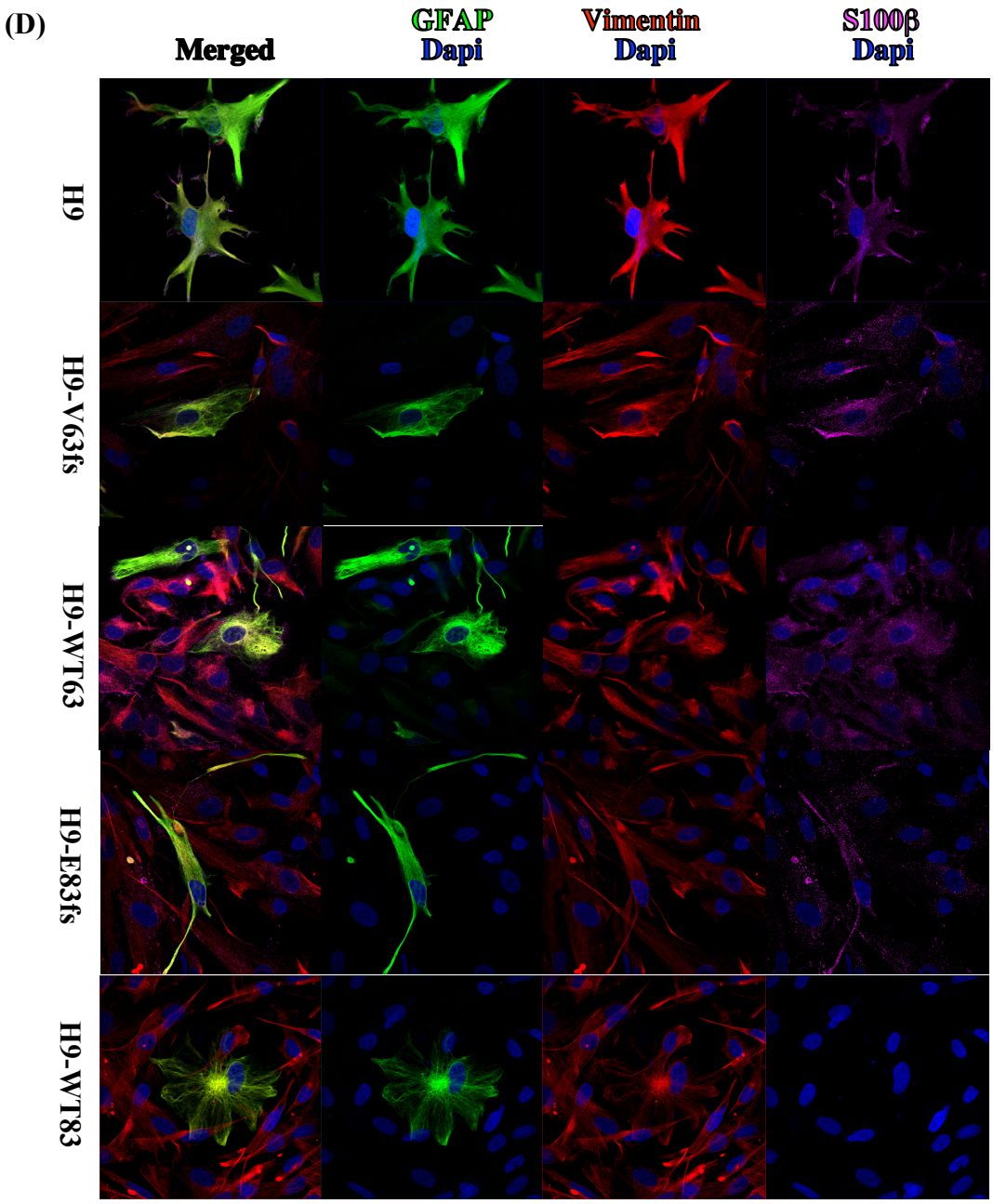

Figure 3. continued

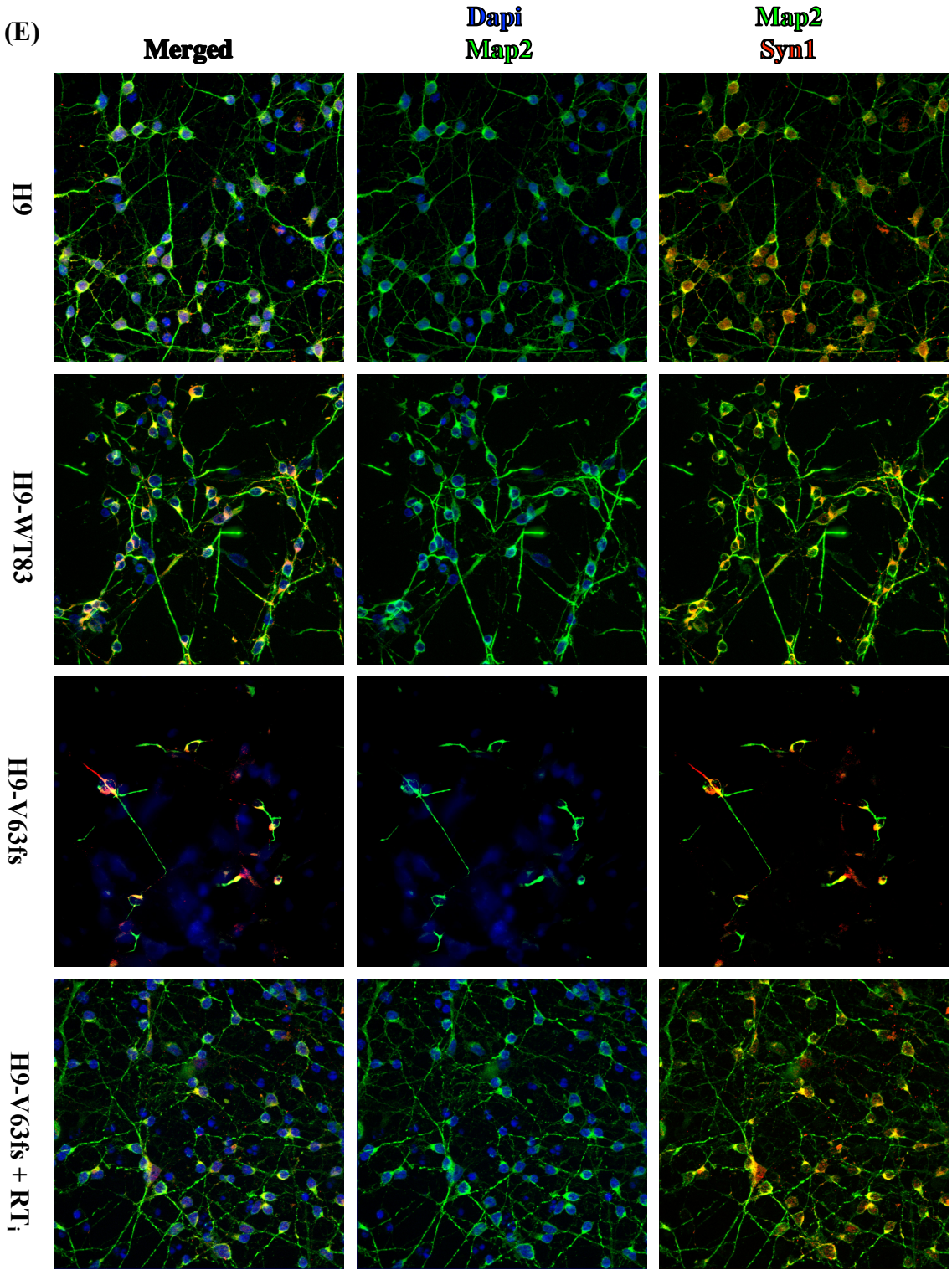

Figure 3. continued

(A)

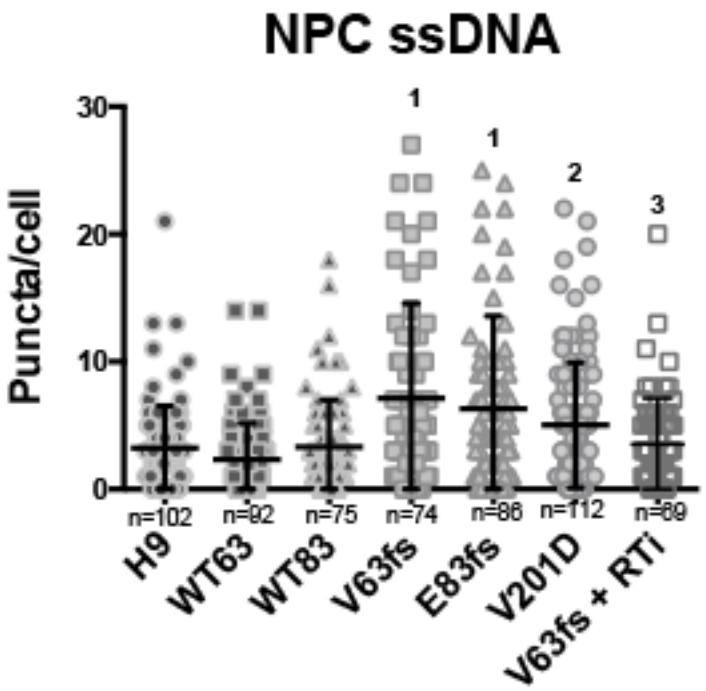

Figure 4. Analysis of AGS nucleic acid (increased ssDNA) phenotype of various cell types with wild-type or mutant TREX1

(A) Quantification of ssDNA puncta in NPCs.
(B) Examples of image from immunocytochemistry of differentiated NPCs to quantify levels of ssDNA in the cytosol. Immunostaining for Nestin (green) and ssDNA (white), as well as the nuclear dapi stain (blue) was performed.
(C) Example of images of stained astrocytes with the V63fs mutation, V63fs astrocytes treated with reverse transcriptase inhibitors, and WT63 astrocytes to quantify levels of ssDNA in the cytosol. Immunostaining for GFAP (green) and ssDNA (white), as well as the nuclear dapi stain (blue) was performed.

(B)

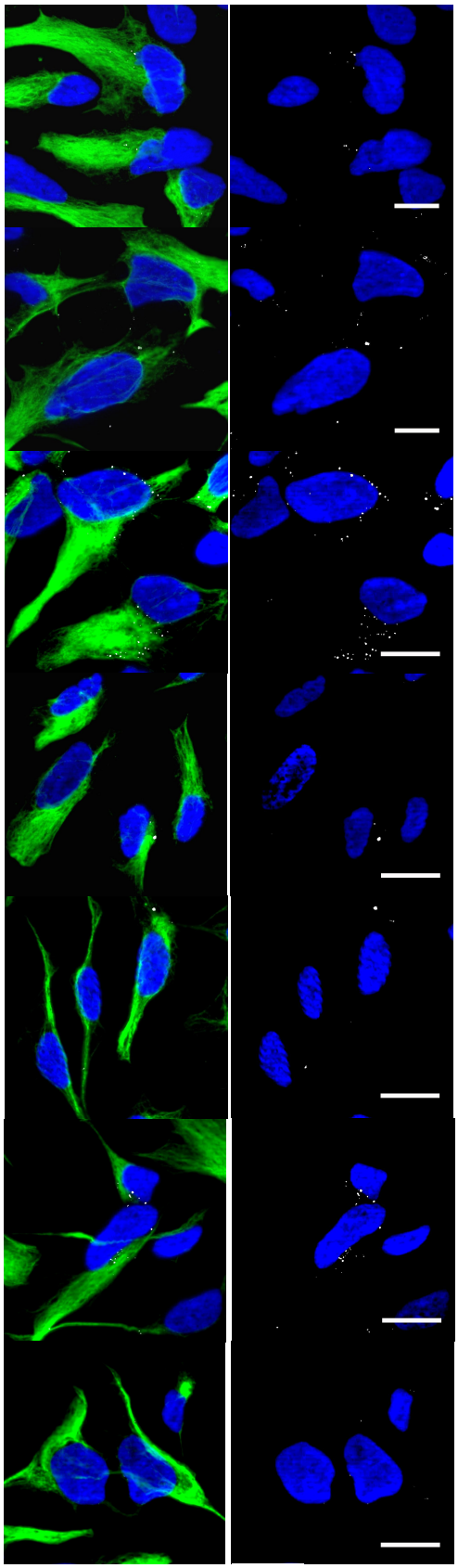

Figure 4. continued

(C)

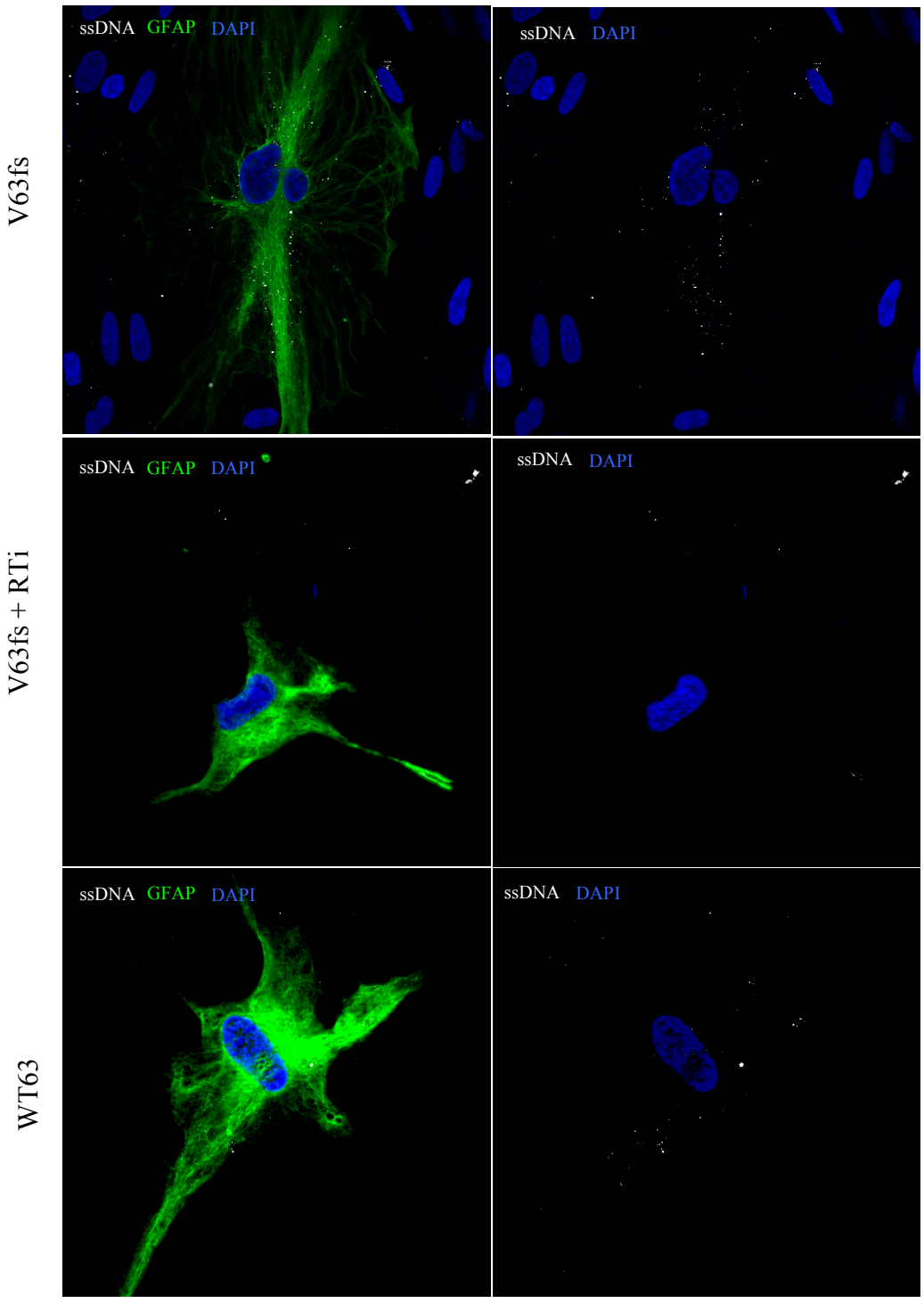

Figure 4. continued

Discussion

When attempting to elucidate the mechanisms that underlie human disease, the accessibility to appropriate disease models is a major factor that dictates the pace at which the field can advance. In neuroscience the rudimentary understanding of the pathology of disease can be attributed not only to the complexity of the nervous system as a whole, but also to the limitations of the current disease models that are in place. In a disease such as Aicardi-Goutières Syndrome in which even animal models don't provide insight on the neurological defects seen in human patients, it is clear that more attention needs to be paid to advancement of the actual platforms for research to be performed. In this work my collaborator, Charles Thomas, and I have begun to develop a new disease model to advance our knowledge of Aicardi-Goutières Syndrome, utilizing the recently developed iPSC technology, as well as new techniques in targeted mutagenesis. The study being presented here has achieved three main goals that yield tremendous utility for advancing our understanding of this disease.

Establishment of isogenic pairs to directly study effects of TREX1 mutations

As discussed previously, two different guide RNAs were used to induce CRISPR/Cas9-mediated mutagenesis by generating site-specific double-stranded breaks and allowing endogenous repair mechanisms to attempt to repair the break. From the 30+ clones isolated from each of the CRISPR/Cas9 treated set of cells, about a quarter of the clones underwent a mutation of some sort, ranging from a single nucleotide insertion or deletion to an insertion of 100 base pairs. While the target sites of the two gRNAs used in this experiment were not at locations in which AGS1 patient mutations are typically seen, the frameshift CRISPR-induced mutations in the selected clones resulted in truncation of the translated mutant TREX1 protein upstream of the catalytic site of the

wild-type TREX1 protein, yielding a loss of the enzymatic function of the protein. This loss of function parallels the biochemical changes seen in AGS1 patients with the V201D mutation, as this missense mutation seen in patients results in a four-fold decrease in TREX1 enzymatic activity.[3] In theory, since the TREX1 WT/MT pairs originate from the same H9 embryonic stem cell line, they are thought to be isogenic besides the single, targeted mutation in TREX1 due to the DNA repair process following the Cas9 nuclease activity. Pairs of cell lines in which the only assumed major difference is a single protein's expression provide the most accurate control/experimental system possible, allowing for direct characterization of the function of that specific protein to help understand its role in disease pathogenesis.

Although mutations in the TREX1 gene were successfully induced as desired, a drawback underlying the CRISPR/Cas9 system for mutagenizing cell lines is the possibility of off-target mutations. With RNA-guided endonucleases that recognize 20bp target sequences and the adjacent PAM sequence, it would be assumed that resulting double-stranded breaks would be unique for a single locus in the genome. It has been seen however, that gRNAs are capable of binding and inducing mutations at sites with up to five mismatched nucleotides at comparable levels to mutations at the target site, generating the possibility of undesired, off-target mutations.[5] Since these additional undesired mutations present extra changes in other genes that could affect our ability to specifically study TREX1, it is necessary to ensure that these off-target mutations are not present. To do this, we have begun exome sequencing to verify that genes with potential off-target sequences have not also been mutagenized. The results from this sequencing are crucial for the integrity of this system as a means to study TREX1 function.

Ability to differentiate pluripotent stem cells into cells of the neural lineage

In this study, I have presented a detailed protocol to produce neural progenitor cells, neurons, and astrocytes from pluripotent embryonic stem cells and induced pluripotent stem cells. While previous groups have described year-long protocols for pluripotent cell differentiation into neurons and astrocytes[15], the protocol developed by the Muotri Lab allows for the formation of $GFAP^+$ astrocytes after about 50 days. The astrocyte cultures developed in this study have a very mixed population of astrocytes with a lower than ideal percentage of GFAP positive cells, therefore we have begun to develop techniques to enhance the purity of astrocyte cultures with GFAP positive cells. By inserting a transgene for tdTomato after the GFAP promoter at the NPC stage, we can purify astrocytes from the non-glial cells after differentiation by FACS based on activity of the GFAP promoter driving the expression for this fluorescent protein. In future experimentation, this enhanced purity will allow for a more homogenous assessment of astrocyte phenotypes.

Similarly, for the differentiation of neurons, we have presented a simple 50 day protocol for neuronal differentiation. As seen in the results presented in this study, the cells developed demonstrate several characteristics of the desired cell type, however a more comprehensive characterization of these differentiated cells must be completed by supplemental experimentation to further explore additional features of each stage of differentiation. Challenges that must be overcome in the differentiation of neurons from neural progenitor cells are the purity and quantity of true neurons. In this study, upon sorting with FACS for cell-surface markers, only a small percentage of the total cells were purified neurons that could be collected for use in further experimentation. In order

to increase the efficiency of this model, increased levels of purified cells per differentiation are necessary.

Since it is very difficult to obtain samples of brain tissue due to high risk for adverse effects, we have presented a technique that, when optimized, will essentially bypass the need for invasive brain biopsies or post-mortem brain tissue when studying particular neurological disorders, expanding our ability to study the disease beyond the radiological and clinical presentations even further.

Production of cells that recapitulate aspects of the AGS phenotype

The value of this model emerges in its ability to recapitulate aspects of the AGS phenotype. Although the bulk of this study focuses on the development of the AGS1 model, some experiments performed provide insight into avenues for exploration in further experimentation. As seen in **Fig. 4**, the cell lines derived in this experiment provide tremendous utility in beginning to examine the different cellular phenotypes of cells in the brain induced by mutations, specifically the changes in cytosolic nucleic acids that are hypothesized to trigger autoimmunity. Due to the need to optimize the differentiation protocols to increase yield of pure cultures, the quantification of ssDNA in neurons and astrocytes was not completed in this study. When these protocols are enhanced and the data is obtained it will provide valuable insight into which cell(s) is/are involved in causing the harmful symptoms of the disease. As shown previously, patients with AGS are seen to have elevated levels of type-1 interferons in the cerebrospinal fluid, presumably due to the deficiency of some sort of nuclease activity.[1] At this point in time, the mechanisms by which these extra endogenous nucleic acids accumulate and the immune response is triggered remain unclear. With the modeled described in this work,

we have created a system in which a targeted approach to studying these unknown components of the disease pathology (and many others) becomes available.

An interesting result seen in this study was the effect of culturing cell lines expressing mutant TREX1 with reverse transcriptase inhibitors (RT_i), starting during the pluripotent stem cell stage. Although an elaborate assessment of the effects of reverse transcriptase inhibitors was not performed, the data seen in the this pilot study suggest a potential role of the process of reverse transcription in formation of the ssDNA thought to trigger cell autoimmunity. As shown in the quantification of ssDNA in NPCs seen in **Figure 4A**, treatment of V63fs NPCs with RT_i resulted in decreased levels of ssDNA when compared to the untreated. Additionally, the differentiated neurons from RT_i treated cell lines showed a sort of rescue of normal neuronal morphology compared to untreated neurons, which showed abnormal morphology and high levels of cell death (not quantified in this study). This observed phenotype may mirror the increased levels of neuronal death seen in AGS patients that result in the cerebral atrophy and microcephaly. With this preliminary observation of a possible benefit to inhibition of reverse transcription, we will explore more specific aspects of the disease phenotype that may improve with treatment to eventually create a therapeutic drug for the disease symptoms.

Although the model prepared here is not necessarily a "disease in a dish model" as some propose, it certainly allows for evaluation of particular phenotypes resulting from genotypic differences. The ability to generate cells of a desired lineage bestows tremendous possibilities for future experimentation, only a few of which were discussed here.

Materials and Methods

Reprogramming of AGS1 patient fibroblasts

AGS1 patient fibroblasts containing a V201D mutation were obtained and sent to the Stem Cell Core at the Sanford Burnham Medical Research Institute for reprogramming using episomal plasmids expressing the Yamanaka factors.

Media composition for all tissue culture

Pluripotent stem cell media (MT): mTeSR™1 (Stem Cell Technologies). Differentiation media for Embryoid Bodies (N2): Dulbecco's Modification of Eagle's Medium/ Ham's F12 (DMEM/F12 50/50; Corning Cellgro©) with 1 x HEPES, 1 x pen-strep, glutamax (Life Technologies), and N2 NeuroPlex™ (Gemini Bio-products). Supplemented with 1μM dorsomorphin (Tocris) and Stemolecule™ SB431542 (StemGent). Neural progenitor cell media (NGF): DMEM/F12 50/50 with 1 x HEPES, 1x pen-strep, glutamax (Life Technologies), N2 NeuroPlex™ (Gemini Bio-products), Gem21 Neuroplex (Gemini Bio-products). Supplemented with 20ng/mL basic fibroblast growth factor (bFGF; R & D). Neuronal media (NG): DMEM/F12 50/50 with 1 x HEPES, 1x pen-strep, glutamax (Life Technologies), N2 NeuroPlex™ (Gemini Bio-products), Gem21 Neuroplex (Gemini Bio-products). Astrocytes were cultured in AGM™ Astrocyte Growth Medium (Lonza).. Treatment with reverse transcriptase inhibitor (RT_i) was with 1μM Stavudine (D4T) and 10μM Lamivudine (3TC).

Maintenance of iPSC and hESC culture

Reprogrammed iPSCs, H9 ESCS, and mutagenized H9 ESCs were propagated in mTeSR™1 and passaged manually onto matrigel (BD Bioscences) coated plates. iPSC passages used for differentiation into NPCs is as follows: passage 18 for A1C1, passages 18 for A1C2, and passages 11 and 13 for A1C3 . ESC passages used for differentiation

into NPCs is as follows: passage 40, 44, and 50 for H9 untransfected, passages 7, 9, 12, and 14 for H9-V63fs (clone 517), passages 11, 14, and 16 for H9-WT63 (clone 521), passages 12, 14, and 15 for H9-E83fs (clone 604), and passages 12, 15, and 17 for H9-WT83 (clone 612).

Purification of mixed cultures of neurons

Neurons were sorted using the BD Influx cell sorter at the Stem Cell Core in the Sanford Consortium for Regenerative Medicine for fluorescence-activated cell sorting (FACS). Neurons were lifted with Accutase and Accumax in FACS Wash Buffer (DPBS, EDTA, HEPES, FBS) passed through a 100μm mesh to break up cells. Cells were spun down and resuspended in a DNase wash (NG media, FBS, DNase) and passed through a 40μm mesh to further separate neurons. The cells were gently spun down again and resuspended in FACS buffer (NG media, FBS, EDTA, and ROCK Inhibitor), with added antibodies for CD24, CD44, and CD184. Cells were incubated in the staining antibody solution in the dark for 30 minutes on ice. Cells were centrifuged and resuspended in FACS buffer and taken to the Stem Cell Core. Cells were sorted and purified neurons with a $CD24^{+}/CD44^{-}/CD184^{-}$ signature were collected every hour for four hours. Purified neurons were plated at a concentration of 100,00 0cells/well on 96 well poly-ornithine/Laminin coated plates.

Immunocytochemistry

Unless otherwise noted, cells were fixed in 4% paraformaldehyde (PFA, Electron Microscopy Sciences) for 20 minutes, washed twice with Dulbecco's Phosphate-Buffered Saline (DPBS ,Corning Cellgro©), permeabilized with 0.25% Triton X-100 for 15 minutes, washed twice with DPBS, blocked with 4% bovine serum albumin (BSA) for an

hour at room temperature, and treated with the primary antibodies diluted in 4% BSA overnight at 4°C. The next day, cells were washed twice with DPBS, incubated with the secondary antibodies (diluted 1:1000 in BSA) for 60 minutes at room temperature, then washed twice, treated with DAPI (diluted 1:10000 in PBS) for five minutes, then washed twice more and mounted. Primary antibody dilutions were used as follows: anti-Nanog (R&D, AF1997, 1:500), anti-Lin28 (Abcam, *ab46020,* 1:500), anti-Nestin (Millipore, *ABD69,* 1:250), anti-Sox2 (Abcam, *ab75485,* 1:250), anti-GFAP (Abcam, *ab4674,* 1:2000), anti-S100β (Abcam, *ab4066,* 1:200), anti-Vimentin (Cell Signaling Technology, *#3932*, 1:50), anti-Map2 (Abcam *ab3392,* 1:2000*)* anti-Syn1 (Millipore *AB1543,* 1:500). Single stranded DNA was stained with anti-ssDNA IgM (Millipore, MAB3299, 1:20). Secondary antibodies conjugated to Alexa Fluors 488, 555, and 647 were used with a dilution of 1:1000 (Life Technologies).

qRT-PCR Transcriptional Analysis

RNA was obtained from cells using by lysing cells in their culture plates using RLT Plus Solution (Qiagen) and 2-mercaptoethanol (500μM). Lysates were collected and homogenized using QiaShredder™ (Qiagen). RNA was collected using an RNeasy Plus Mini Kit (Qiagen). One microgram of RNA used to make cDNA using Qiagen's Quantitect Reverse Transcriptase Kit. One nanogram of cDNA was used in qPCR analysis of gene expression using TaqMan probes with Taqman Universal Master Mix II (Life Technologies). Reactions were performed in triplicate and average C_q and SEM values were reported.

Single stranded DNA (ssDNA) quantification

Cells used for ssDNA analysis were fixed with cold 4% PFA for 20 minutes and then incubated in 80% methanol overnight. Cells were washed twice with DPBS then treated with RNASE1 in S1 Nuclease Buffer for four hours at 37°C. Cells were washed with DPBS, blocked with BSA at room temperature for an hour, then stained with the antibodies described previously. Cover slips were mounted onto glass slides and the identities of the cells on each slide were replaced by an additional person assigning letters to each slide, ensuring no bias was performed when capturing images. A Zeiss Apotome fluorescence microscope was used to capture ten 100x images of each cell line. ssDNA puncta were quantified by measuring puncta per cell (as determined by the nuclear dapi stain), still without knowledge of the identity of the cells each image represented.

References

1. Ablasser, Andrea, Inga Hemmerling, Jonathan L. Schmid-Burgk, Rayk Behrendt, Axel Roers, and Veit Hornung. "TREX1 Deficiency Triggers Cell-Autonomous Immunity in a CGAS-Dependent Manner." *The Journal of Immunology* 192.12 (2014): 5993-997. Web.

2. Crow, Yanick J. "Summary." *Aicardi-Goutières Syndrome*. U.S. National Library of Medicine, 13 Mar. 2014. Web. 11 May 2014.

3. Crow, Yanick J., Bruce E. Hayward, Rekha Parmar, Peter Robins, Andrea Leitch, Manir Ali, Deborah N. Black, Hans Van Bokhoven, Han G. Brunner, Ben C. Hamel, Peter C. Corry, Frances M. Cowan, Suzanne G. Frints, Joerg Klepper, John H. Livingston, Sally Ann Lynch, Roger F. Massey, Jean François Meritet, Jacques L. Michaud, Gerard Ponsot, Thomas Voit, Pierre Lebon, David T. Bonthron, Andrew P. Jackson, Deborah E. Barnes, and Tomas Lindahl. "Mutations in the Gene Encoding the 3′-5′ DNA Exonuclease TREX1 Cause Aicardi-Goutières Syndrome at the AGS1 Locus." *Nature Genetics* 38.8 (2006): 917-20. Web.

4. Fazzi, Elisa, Marco Cattalini, Simona Orcesi, Angela Tincani, L. Andreoli, U. Balottin, M. De Simone, M. Fredi, F. Facchetti, J. Galli, S. Giliani, A. Izzotti, A. Meini, I. Olivieri, and A. Plebani. "Aicardi–Goutieres Syndrome, a Rare Neurological Disease in Children: A New Autoimmune Disorder?" *Autoimmunity Reviews* 12.4 (2013): 506-09. Web.

5. Fu, Yanfang, Jennifer A. Foden, Cyd Khayter, Morgan L. Maeder, Deepak Reyon, J. Keith Joung, and Jeffry D. Sander. "High-frequency Off-target Mutagenesis Induced by CRISPR-Cas Nucleases in Human Cells." *Nature Biotechnology* 31.9 (2013): 822-26. Web.

6. Hou, Z., Y. Zhang, N. E. Propson, S. E. Howden, L.-F. Chu, E. J. Sontheimer, and J. A. Thomson. "Efficient Genome Engineering in Human Pluripotent Stem Cells Using Cas9 from Neisseria Meningitidis." *Proceedings of the National Academy of Sciences* 110.39 (2013): 15644-6649 15644-5649. Web.

7. Kavanagh, David, Dirk Spitzer, Parul Kothari, Aisha Shaikh, M. Kathryn Liszewski, Anna Richards, and John P. Atkinson. "New Roles for the Major Human 3′-5′ Exonuclease TREX1 in Human Disease." *Cell Cycle* 7.12 (2008): 1718-725. Web.

8. Lehtinen, D. A., S. Harvey, M. J. Mulcahy, T. Hollis, and F. W. Perrino. "The TREX1 Double-stranded DNA Degradation Activity Is Defective in Dominant

Mutations Associated with Autoimmune Disease." *Journal of Biological Chemistry* 283.46 (2008): 31649-1656. Web.

9. Liu, K., Y. Song, H. Yu, and T. Zhao. "Understanding the Roadmaps to Induced Pluripotency." *Cell Death and Disease* 5.E1232 (2014). Web.

10. Mali, Prashant, Kevin M. Esvelt, and George M. Church. "Cas9 as a Versatile Tool for Engineering Biology." *Nature Methods* 10.10 (2013): 957-63. Web.

11. Namjou, B., P. H. Kothari, J. A. Kelly, S. B. Glenn, J. O. Ojwang, A. Adler, M. E. Alarcón-Riquelme, C. J. Gallant, S. A. Boackle, L. A. Criswell, R. P. Kimberly, E. Brown, J. Edberg, A. M. Stevens, C. O. Jacob, B. P. Tsao, G. S. Gilkeson, D. L. Kamen, J. T. Merrill, M. Petri, R. R. Goldman, L. M. Vila, J-M Anaya, T. B. Niewold, J. Martin, B. A. Pons-Estel, J. M. Sabio, J. L. Callejas, T. J. Vyse, S-C Bae, F. W. Perrino, B. I. Freedman, R. H. Scofield, K. L. Moser, P. M. Gaffney, J. A. James, C. D. Langefeld, K. M. Kaufman, J. B. Harley, and J. P. Atkinson. "Evaluation of the TREX1 Gene in a Large Multi-ancestral Lupus Cohort." *Genes and Immunity* 12.4 (2011): 270-79. Web.

12. Rice, Gillian, Teresa Patrick, Rekha Parmar, Claire F. Taylor, Alec Aeby, Jean Aicardi, Rafael Artuch, Simon Attard Montalto, Carlos A. Bacino, Bruno Barroso, Peter Baxter, Willam S. Benko, Carsten Bergmann, Enrico Bertini, Roberta Biancheri, Edward M. Blair, Nenad Blau, David T. Bonthron, Tracy Briggs, Louise A. Brueton, Han G. Brunner, Christopher J. Burke, Ian M. Carr, Daniel R. Carvalho, Kate E. Chandler, Hans-Jürgen Christen, Peter C. Corry, Frances M. Cowan, Helen Cox, Stefano D'Arrigo, John Dean, Corinne De Laet, Claudine De Praeter, Catherine Déry, Colin D. Ferrie, Kim Flintoff, Suzanna G.m. Frints, Angels Garcia-Cazorla, Blanca Gener, Cyril Goizet, Françoise Goutières, Andrew J. Green, Agnès Guët, Ben C.j. Hamel, Bruce E. Hayward, Arvid Heiberg, Raoul C. Hennekam, Marie Husson, Andrew P. Jackson, Rasieka Jayatunga, Yong-Hui Jiang, Sarina G. Kant, Amy Kao, Mary D. King, Helen M. Kingston, Joerg Klepper, Marjo S. Van Der Knaap, Andrew J. Kornberg, Dieter Kotzot, Wilfried Kratzer, Didier Lacombe, Lieven Lagae, Pierre Georges Landrieu, Giovanni Lanzi, Andrea Leitch, Ming J. Lim, John H. Livingston, Charles M. Lourenco, E. G. Hermione Lyall, Sally A. Lynch, Michael J. Lyons, Daphna Marom, John P. Mcclure, Robert Mcwilliam, Serge B. Melancon, Leena D. Mewasingh, Marie-Laure Moutard, Ken K. Nischal, John R. Østergaard, Julie Prendiville, Magnhild Rasmussen, R. Curtis Rogers, Dominique Roland, Elisabeth M. Rosser, Kevin Rostasy, Agathe Roubertie, Amparo Sanchis, Raphael Schiffmann, Sabine Scholl-Bürgi, Sunita Seal, Stavit A. Shalev, C. Sierra Corcoles, Gyan P. Sinha, Doriette Soler, Ronen Spiegel, John B.p. Stephenson, Uta Tacke, Tiong Yang Tan, Marianne Till, John L. Tolmie, Pam Tomlin, Federica Vagnarelli, Enza Maria Valente, Rudy N.a. Van Coster, Nathalie Van Der Aa, Adeline Vanderver, Johannes S.h. Vles, Thomas Voit, Evangeline Wassmer, Bernhard Weschke, Margo L. Whiteford, Michel A.a. Willemsen,

Andreas Zankl, Sameer M. Zuberi, Simona Orcesi, Elisa Fazzi, Pierre Lebon, and Yanick J. Crow. "Clinical and Molecular Phenotype of Aicardi-Goutières Syndrome." *The American Journal of Human Genetics* 81.4 (2007): 713-25. Print.

13. Silva, U. De, S. Choudhury, S. L. Bailey, S. Harvey, F. W. Perrino, and T. Hollis. "The Crystal Structure of TREX1 Explains the 3' Nucleotide Specificity and Reveals a Polyproline II Helix for Protein Partnering." *Journal of Biological Chemistry* 282.14 (2007): 10537-0543. Web.

14. Takahashi, Kazutoshi, and Shinya Yamanaka. “Induction of Pluripotent Stem cells from Mouse Embryonic and Adult Fibroblast Cultures by Defined Factors.” *Cell* 126.4 (2006): 663-76. Web.

15. Williams, Emily C., Xiaofen Zhong, Ahmed Mohamed, Ronghui Li, Yan Liu, Qiping Dong, Gene E. Ananiev, Jonathan C. Mok, Benjamin R. Lin, Jianfeng Liu, Cassandra Chiao, Rachel Cherney, Hongda Li, Su-Chun Zhang, and Qiang Chang. "Mutant Astrocytes Differentiated from Rett Syndrome Patients-specific IPSCs Have Adverse Effects on Wild-type Neurons." *Human Molecular Genetics* 23.11 (2014): 2968-980. Web.

16. Yu, J., K. Hu, K. Smuga-Otto, S. Tian, R. Stewart, I. I. Slukvin, and J. A. Thomson. "Human Induced Pluripotent Stem Cells Free of Vector and Transgene Sequences." *Science* 324.5928 (2009): 797-801. Web.

17. Zhang, Feng, Yan Wen, and Xiong Guo. "CRISPR/Cas9 for Genome Editing: Progress, Implications and Challenges." *Human Molecular Genetics* (2014): n. pag. Web.